Smart Structures and Systems, *Vol. 30, No. 5 (2022) 479-500*
https://doi.org/10.12989/sss.2022.30.5.479

Seismic control of high-speed railway bridge using S-shaped steel damping friction bearing

Wei Guo*[1,2], Yang Wang [1,2a], Zhipeng Zhai [3] and Qiaodan Du [1]

[1] *School of Civil Engineering, Central South University, Changsha, China*
[2] *National Engineering Research Center of High-Speed Railway Construction Technology, Changsha, China*
[3] *Earthquake Engineering Research and Test Center, Guangzhou University, Guangzhou, China*

(*Received November 14, 2021, Revised August 9, 2022, Accepted August 25, 2022*)

Abstract. In this study, a new type of isolation bearing is proposed by combining S-shaped steel plate dampers (SSDs) with a spherical steel bearing, and the seismic control effect of a five-span standard high-speed railway bridge is investigated. The advantages of the proposed S-shaped steel damping friction bearing (SSDFB) are that it cannot only lengthen the structural periods, dissipate the seismic energy, but also prevent bridge unseating due to the restraint effectiveness of SSDs in the large relative displacements between the girders and piers. This study first presents a detailed description and working principle of the SSDFB. Then, mechanical modeling of the SSDFB was derived to fundamentally define its cyclic behavior and obtain key mechanical parameters. The numerical model of the SSDFB's critical component SSD was verified by comparing it with the experimental results. After that, parameter studies of the dimensions and number of SSDs, the friction coefficient, and the gap length of the SSDFBs were conducted. Finally, the longitudinal seismic responses of the bridge with SSDFBs were compared with the bridge with spherical bearing and spherical bearing with strengthened shear keys. The results showed that the SSDFB can not only significantly mitigate the shear force responses and residual displacement in bridge substructures but also can effectively reduce girder displacement and prevent bridge unseating, at a cost of inelastic deformation of the SSDs, which is easy to replace. In conclusion, the SSDFB is expected to be a cost-effective option with both multi-stage energy dissipation and restraint capacity, making it particularly suitable for seismic isolation application to high-speed railway bridges.

Keywords: combination energy dissipation; flexural-tensile behavior; high-speed railway bridge; isolation bearing; numerical modelling; seismic control; S-shaped steel damper

1. Introduction

To improve the running safety and stability of high-speed trains (HSTs), more than half of high-speed railway (HSR) lines in China adopt bridges (He *et al*. 2017), and the majority of which are simply supported bridges (SSBs) (Zhai and Xia 2001). As HSR lines are extending to seismic-prone regions, the bridges are exposed to greater seismic risk. Due to the large cross-sections of HSR girders, and together with the additional mass of the track structure, the inertia forces of the superstructure that transmitted to the piers are large under high-level earthquakes (Li *et al*. 2021). Besides, the HSR piers generally have a lower longitudinal reinforcement ratio, which results in a lower ductility and energy dissipation capacity (Shao *et al*. 2014). Shake table test shows that HSR piers that fix connect to girders are expected to sustain irreparable damage given an earthquake of 0.50 g peak ground acceleration (PGA) especially for piers with unequal height (Kang *et al*. 2017). Meanwhile, the fixed bearings are also vulnerable due to excessive inertia force of superstructures (Filipov *et al*. 2013, Jangid and Kelly 2001), which are hard to replace after the fix bearing slides.

The structural damages of HSR bridges illustrate that current force-based methodology in railway seismic design codes (TB 10621-2014, GB 50111-2006) mainly focus on the prevention from structure collapse using the hysteretic plastic deformation and high-stiffness of structural components, and not well considered the bridge seismic resilience. As energy-dissipated components are usually a part of the gravity-resisting system, repair of damaged components after an earthquake is often difficult and expensive (Guo *et al*. 2022, Zou *et al*. 2019), which will inevitably affect the traffic function of HSR lines. Thus, mitigating seismic structural damage and improving post-earthquake recoverability of HSR bridges is important for the timely and cost-effectively opening of the HSR lines. Various types of control methods, such as active, semi-active, and passive have been developed to minimize the bridge structural damage and enhancing seismic resilience (Lin *et al*. 2018, Hwang *et al*. 2020). Among these methods, the passive control devices are more practical due to their easy implementation and low cost (Martinez and Filiatrault 2015). There are two general categories of passive control methods including (a) seismic isolators that reduce the energy input to a structure by avoiding the seismic dominant frequencies and (b) energy dampers which

*Corresponding author, Ph.D., Professor,
E-mail: guowei@csu.edu.cn
[a] Ph.D. Student, E-mail: wycivil@csu.edu.cn

ISSN: 1738-1584 (Print), 1738-1991 (Online)

dissipate the input energy through hysteretic responses of elastoplastic materials (AASHTO 2014).

Since the HSR bridges are generally possessed high natural frequencies due to their large stiffness, the bridge periods would be largely enlarged when the isolator bearings start functioning, thus the shear forces of piers in turn are reduced. However, considering the safety and stability of HST, the performance of HSR bridge bearing should have strict requirements (Zou *et al*. 2019), and the commonly used isolation bearings may be difficult to meet the requirements. Lead rubber bearings have been used in a lot of highway bridges due to their good energy dissipation (Patrick *et al*. 2017). However, their vertical bearing capacities are inadequate for HSR bridges (Guan *et al*. 2010). Friction pendulum bearings have large bearing capacity and self-resetting function. But the girder's gravity center gets raised while friction pendulum bearings are adopted, which is detrimental to upper track structures (Li *et al*. 2021). Therefore, many researches were focusing on the isolation effects of the common-used spherical and pot bearings in railway bridges. Jiang *et al*. (2019) investigated the influence of friction coefficient on spherical bearing's isolation behavior: a smaller friction coefficient leads to smaller pier forces but larger relative displacements between pier and girder. Wei *et al*. (2017) found that the sliding action of fixed spherical bearings reduce the inertia force and decrease the seismic vulnerability of piers.

Several improvements have been proposed with the goal of dissipating seismic energy while providing seismic isolation in the bearing. Zou *et al*. (2019) proposed a new isolation design with a function separation concept by integrating the sliding friction bearing and lead rubber bearing together. Feng *et al*. (2020) adopted the E-shaped steel damping bearing (ESSDB) in railway extradosed bridge. Meanwhile, other elastoplastic isolation bearing similar to the ESSDB have been developed and applied, e.g., utilizing X-shaped (Xiang and Li 2016), C-shaped (Sheikhi *et al*. 2021), dual-ring dampers (Mahdi *et al*. 2021) and triangular dampers (Shen *et al*. 2017). The elastoplastic steel dampers have proven advantages of stable hysteretic characteristics, high damping effects, and easy replacement (Mohsen *et al*. 2021). Under design-level and high-level earthquakes, the steel dampers are to yield and dissipate input energy by hysteretic behavior, and thus forces transmitted to bridge substructures are reduced. After high-level earthquakes, only the steel dampers need to be replaced, with no or minimal damage to other structural components. But while adopting isolate bearings, the horizontal stiffness between girders and piers will inevitably weaken, and the relative displacements of the girders and piers will increase, which can lead to the unseating of bridge spans or even collapse (Li *et al*. 2008, Raheem 2009, Kawashima *et al*. 2011). For HSR bridges, the large relative displacement of the girders and piers may cause damages to the ballastless track structure (Guo *et al*. 2020a, c), also increasing the possibility of derailment (He *et al*. 2011, Luo 2005). To reduce the risk of collapse due to unseating, restrainers are commonly used to retrofit the bridges, for limiting the relative displacement of the bridge and pier (Yuan *et al*. 2012, Li *et al*. 2018). However, the bridge restrainers, no matter cable or spring type (Guo *et al*. 2017), are difficult to design for providing adequate seating widths to prevent span collapse, while at the same time mitigating the seismic response of the piers (Li *et al*. 2008). In recent years, the flexural-tensile steel dampers have been investigated and the results show that their secondary stiffness and strength gradually increased due to steel's tensile strengthening effect (Mohsen *et al*. 2021). The S-shaped steel damper (SSD) proposed by our group (Zhai *et al*. 2020) consists of S-shaped plates made of common steel, which are easy to manufacture, install and replace. The SSD was implemented in building structures, and the result shows: when the displacement is medium, input energy is dissipated by flexural elastoplastic deformation of the steel plate; when the displacement is large, the deformation shifts from flexural to tensile behavior. These characteristics may also suitable for bridges as an energy dissipatedly restrainer.

Based on the above, an innovative hybrid isolate bearing was proposed by combining the steel spherical bearing and the SSDs to achieve energy dissipation and displacement restrain capacities. The working behavior of S-shaped steel damping friction bearing (SSDFB) was first investigated. Then by comparing with cyclic test results and obtained theoretical curves, the accuracy of the numerical model in ABAQUS was verified. Based on the established numerical model, the influences of key bearing parameters on the SSDFB mechanical characteristics were investigated. After that, a 5-span HSR bridges model adopting the SSDFB was built in OpenSees software. Finally, longitudinal seismic performance of the SSDFB isolated bridge was evaluated corresponding to a normal and strengthen spherical bearing configuration.

2. Description of the S-shaped steel damping friction bearing

2.1 Description of the SSDFB

The ideal isolation bearing should have at least two basic functions: the first is bearing function and the second is isolation function with energy dissipation. In the normal working stage, the bearings should ensure vertical bearing, rotation, horizontal movement, and other functions which can guarantee the normal usages of railway bridges (Zou *et al*. 2019). When an earthquake strikes, the bridge structure is subjected to dynamic oscillations of larger periods and the seismic energy is dissipated by friction, metal yielding, or viscous damping, etc. Fig. 1 shows the conceptual schematic view of the proposed isolation bearing in this study. Here, a hybrid isolate bearing is proposed by combining the spherical steel bearing commonly used in railway bridges (Jiang *et al*. 2019) which has good frictional energy dissipation capability and SSDs with features of large secondary stiffness, high over-strength factor and stable flexural-tensile behavior (Zhai *et al*. 2020). Thus, the proposed SSDFB combines two types of energy dissipation methods with multi-stage energy dissipation characteristics and has a strong restraining function.

The SSDFBs can be divided into fixed bearing and movable bearing by whether allowing relative movement of

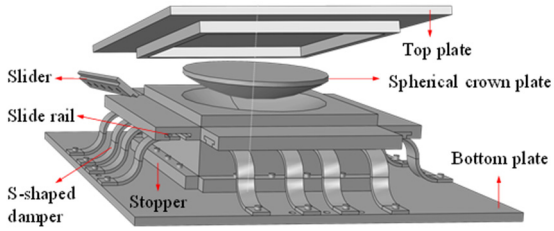

Fig. 1 The proposed S-shaped steel damping friction bearing

girders and piers at normal working stage. Basic configurations of the fixed and movable SSDFB are shown in Fig. 2. The fixed and movable directions of SSDFB are mapped to the bridge coordinates in Fig. 17. The proposed SSDFB has the following structural modifications while maintaining the basic components of the spherical bearing:

- Four slide rails are attached to the edge of the middle plate. To ensure wear resistance and reduce its friction coefficient, the slide rails are covered with a layer of ultra-high molecular weight polyethene (UHMW-PE). When the bearing moves along the slide rails, the SSDs in the other direction will not deform out-of-plane. A layer of UHMW-PE is also bonded to the plate end that is in contact with the stoppers, which allow stoppers orthogonal to the moving direction to provide lateral support but does not impede sliding.
- The SSDFB, consisting of an adjustable number of SSDs, whose upper end is connected to the slider, and the lower end is fixed to the bottom plate utilizing bolts so that the steel damper can be easily replaced when it is damaged under strong earthquakes.
- In the fixed direction of the bearing, the shear key is connected to the stopper providing a large stiffness. When the seismic force exceeds limit, the shear key is sheared off and the bearing starts to slide. After that, the additional friction surface (AFS) starts dissipating energy by friction.
- In the movable direction of the bearing, a gap is left between the side of the upper plate and the middle plate to meet the deformation of girders. A layer of rubber bedding is pasted on the side of the upper plate to cushion the contact with the middle plate under earthquakes.

2.2 Working principle

The SSDFB integrates frictional energy dissipation of the AFS and plastic energy dissipation of SSD. The movable bearing enters the slide working state when the relative displacement of the girder and pier exceeds the gap of movable bearings, and the seismic force exceeds the friction limit of the AFS. Since the initial stiffness of SSD is relatively small, it enters flexural plastic deformation stage subsequently. As the seismic force increases till the shear key shears off, the fixed bearing also enters the slide dissipating working state, which leads to the decreasing of the bridge structure horizontal stiffness and enlarging of the structural period. Meanwhile, fixed bearings also dissipate seismic energy through friction and plastic deformation of SSDs after shear key's damage. For the entire bridge structure, the combination of movable and fixed bearings can achieve graded energy dissipation at different seismic intensities. In large displacement, the flexural deformation of SSD transforms to tensile behavior. Therefore, the SSD has large secondary stiffness and a high over-strength factor. Thus, higher stiffness and strength under strong earthquakes can be provided. This effect is like that of the 'cable' used as bridge restrainers (Yuan *et al*. 2012), which have a strong limiting effect to prevent the bridge from bridge falling.

2.3 Mechanical modeling of the SSDFB

Based on their physical composition described in section 2.1, mechanical models SSDFBs are proposed here. The mechanical model of the fixed bearing consists of the SSD, AFS and shear key unit in parallel, as shown in Fig. 3(a). The mechanical model of the movable bearing is shown in Fig. 3(b), which uses an assembly of a plane slider in series with the parallel system of an SSD and an AFS. The movement range of the plane slider is limited between the gap.

The shear key unit in the fixed bearing has a fragile failure mode, and its backbone curve is shown in Fig. 4(a): the shear key breaks as the shear force exceeds the shear key's limit shear force F_s, then the horizontal support force is rapidly reduced to zero. The corresponding limit shear displacement of the shear key is d_s. The friction behaviors of the AFS and the plane slider are simulated using the Coulomb friction model, whose mechanical behavior is a bilinear model of ideal elastoplastic, as shown in Fig. 4(b). The friction yield displacement of the AFS is d_f, and the friction yield displacement of plane slider is d_{fp}. In Fig.

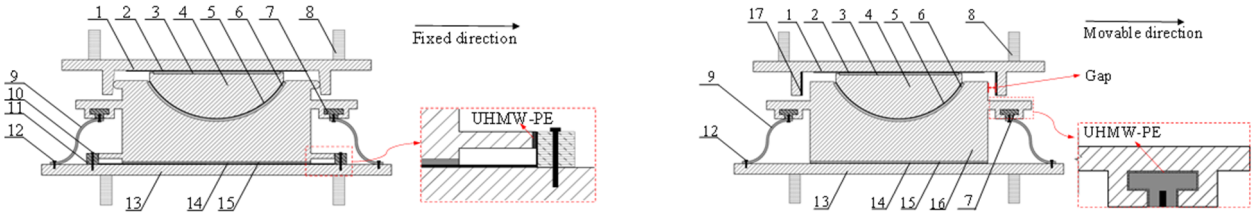

(a) Fixed bearing (b) Movable bearing

Fig. 2 Basic configurations of the fixed and movable SSDFB

(a) Fixed bearing (b) Movable bearing

Fig. 3 Mechanical model of the SSDFB

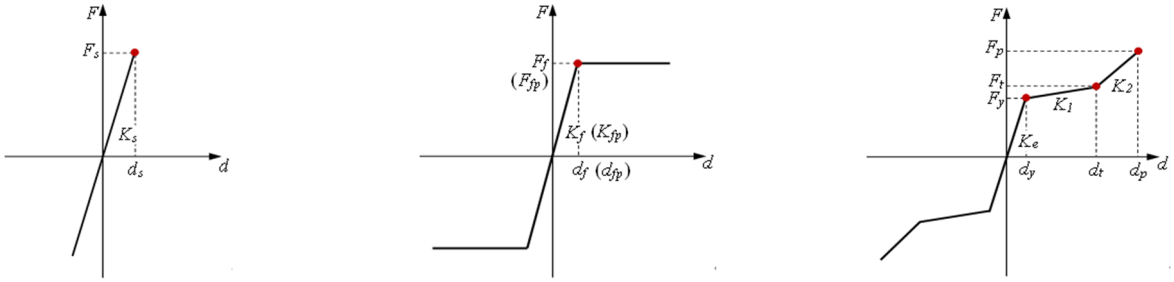

(a) Shear key (b) Friction plate (c) S-shaped steel damper

Fig. 4 Backbone curves of SSDFB's components

(a) Top view (b) Side view

Fig. 5 Dimension of S-shaped steel plate

4(b), F_f represents the sliding friction force of the additional friction plate, F_{fp} represents the sliding friction force of the plane slider. By multiplying the friction coefficient and the vertical force, the following equations of friction force are given: $F_f = \mu N$ and the $F_{fp} = \mu_p N$, where μ donates the friction coefficient of the AFS, μ_p means the friction coefficient of the plane slider, N represents the vertical load from superstructure of bridge.

The geometric configuration of S-shaped steel plate is shown in Fig. 5, where b is the steel plate width, l represents the top and bottom end length of the plate, d denotes the bolt hole's diameter, D means the height of the damper and t is the plate thickness. The SSD's backbone curve is represented by the proposed multi-linear force-displacement model, which was validated by cyclic experimental results (Zhai *et al.* 2020). Notably, the SSD is proven to possess good seismic control effects in buildings but has not applied in bridges yet and its seismic performance in HSR bridges is not clear. Fig. 4(b) specifies several key parameters, including the initial stiffness K_e, the yielding displacement d_y and force F_y, the first yielding stiffness K_1, the second yielding displacement d_t and force F_t, the second yielding stiffness K_2, the peak force F_p and displacement d_p at tensile strengthening stage. Also, due to the tensile behavior of the SSD, K_2 is much larger than K_1.

The relationship between multi-linear force-displacement model key parameters and dimensions of SSD are fitted from experimental and numerical results (Zhai *et al.* 2020), which are given as following equations

$$d_y = 1.94\frac{\sigma_y t}{E}(D/t-1)^{1.58} \quad (1)$$

$$K_e = 2.39Eb(D/t-1)^{-2.63} \quad (2)$$

$$d_p = 163.38d_y(D/t)^{-0.75} \quad (3)$$

$$F_p = 0.96\sigma_y bt \quad (4)$$

$$K_1 = 0.001K_e(D/t)^{1.5} \quad (5)$$

$$K_2 = 5.97\times10^{-5}K_e(D/t)^{2.88} \quad (6)$$

where E is the modulus of elasticity of the steel, σ_y is the yield stress of the steel.

For the fixed bearings, the limit shear displacement of the shear key, the friction yield displacement of the additional friction plate, and the friction yield displacement

of plane slider are all quite small compared to the bearing's overall movement (Jiang *et al*. 2019) and can be designed to be the same, i.e., $d_s = d_f = d_{fp}$. Since d_y is larger than d_s, the SSD's stiffness is still equal to the initial stiffness K_e. Thus, the initial stiffness of fixed bearing and yield force are given as follows

$$K_{G1} = F_s/d_s + F_f/d_f + K_e = K_s + K_f + K_e \tag{7}$$

$$F_{Gy} = F_s + F_f + K_e d_s = K_{G1} d_s \tag{8}$$

For the movable bearings, when the bearing's slide distance exceeds the gap length d_g, while the seismic force exceeds the bearing's slide yield force F_{Hy}, the additional plate along with the SSD start dissipating together. The formular of F_{Hy} is shown below

$$F_{Hy} = F_f + K_e d_f \tag{9}$$

The four-stage force-displacement relationship of fixed and movable SSDFBs is given in Eq. (10), through the above mechanical model of SSDFB's components and their connections. As the shear key is only functional in normal working stage (stage I), and this study is mostly concerned with the seismic isolation performance of the bearings under earthquake, so the initial stiffness of fixed bearing can be simplified from K_{G1} to $K_f + K_e$. The mechanical model of the fixed SSDFB in the loading process are shown in Fig. 6(a) and several key points are specified here.

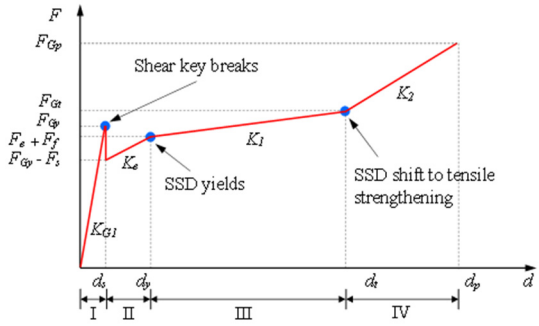

(a) Fixed bearing

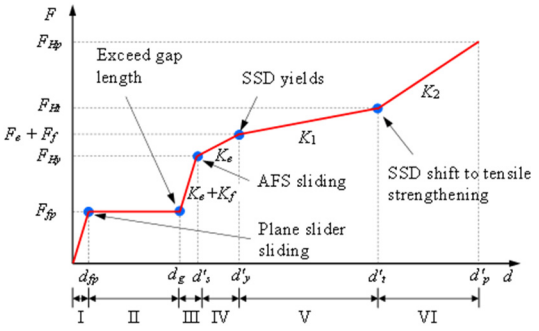

(b) Movable bearing

Fig. 6 Mechanical model of the SSDFB in the loading process

$$F_G = \begin{cases} K_{G1} d & (0 \le d < d_s) \quad \text{Stage I} \\ F_{Gy} - F_s + K_e(d - d_s) & (d_s \le d < d_e) \quad \text{Stage II} \\ F_e + F_f + K_1(d - d_e) & (d_e \le d < d_t) \quad \text{Stage III} \\ F_e + F_f + K_1 d_t + K_2(d - d_t) & (d_t \le d < d_p) \quad \text{Stage IV} \end{cases} \tag{10}$$

Similarly, the six-stage force-displacement relationship is given in Eq. (11) and the corresponding mechanical model with key points of the movable SSDFB in the loading process are shown in Fig. 6(b), in which the $d'_s = d_s + d_g$, $d'_y = d_y + d_g$, $d'_t = d_t + d_g$, $d'_p = d_p + d_g$.

$$F_H = \begin{cases} K_{fp} d & (0 \le d < d_{fp}) \quad \text{Stage } I \\ K_{fp} d_{fp} = F_{fp} & (d_{fp} \le d < d_g) \quad \text{Stage II} \\ F_{fp} + (K_e + K_f)(d - d_g) & (d_g \le d < d_g + d_s) \quad \text{Stage III} \\ F_{Hy} + K_e(d - d_g - d_s) & (d_g + d_s \le d < d_g + d_e) \quad \text{Stage IV} \\ F_e + F_f + K_1(d - d_g - d_e) & (d_g + d_e \le d < d_g + d_t) \quad \text{Stage } V \\ F_e + F_f + K_1 d_t + K_2(d - d_g - d_t) & (d_g + d_t \le d < d_g + d_p) \quad \text{Stage VI} \end{cases} \tag{11}$$

3. Numerical model of SSDFB and parametric studies

In section 2, the theoretical force-displacement relationships of SSDFB are proposed. Finite element (FE) software such as ABAQUS have been proven to have sufficient analytical accuracy to meet the requirements of engineering calculations (Guo *et al*. 2021, Zhai *et al*. 2020). This section uses ABAQUS to establish the refined FE model of the SSDFB, and the simulation accuracy of the SSDFB's critical component SSD was verified by experimental results. Meanwhile, the theoretical curves of the entire SSDFB are compared with the numerical force-displacement results.

3.1 Finite element model of SSDFB

3.1.1 FE model verification of SSD

The materials in the SSDFB mainly contain Q345 steel, Q235 steel and UHMW-PE (GB/T 1591 2008), among which the upper plate, spherical crown plate, middle plate, slide rail, slider and lower plate of the bearing are made of Q345 steel, the SSD is made of Q235 steel with lower yield strength. The SSDFB mainly dissipates energy through

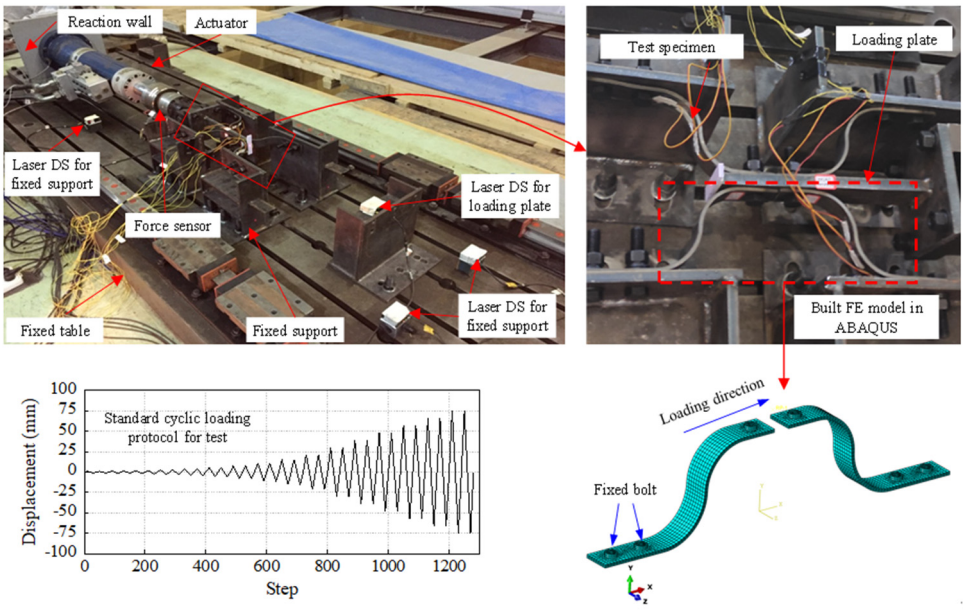

Fig. 7 Test setup and numerical model for test specimens

SSDs and the sliding friction, among which the mechanical behavior of the SSD is more complex, and the accuracy of SSD's numerical model significantly affects the simulation accuracy of the SSDFB's FE model. The force-displacement relationship of the spherical bearing has been studied in detail in the literature (Jiang *et al*. 2019). Major components of the commonly used spherical steel bearing are usually in a small stress state. Therefore, in this study, unidirectional static loading tests were conducted on the SSDs. Fig. 7 shows the test setup, in which the test specimens were connected to four fixed supports using bolts and a rigid loading plate that connected to the actuator. For the symmetry of forward and backward loading, two SSDs were arranged on each side of the loading plate.

To study the seismic performance of SSD, two specimens with different heights D were tested. The height D for specimen 1 and for specimen 2 is 108 mm and 133 mm, respectively. The width b, the plate thickness t, the end plate's length l, and diameter of the bolt hole d are equal for the two test specimens, which are 40 mm, 5 mm, 100 mm and 18 mm, respectively. The tests were conducted utilizing the hydraulic uniaxial actuator with 70 kN loading capacity in the High-Speed Railway Construction National Engineering Research Center, which is shown in Fig. 7 (Zhai *et al*. 2020). The high strength bolts with 900 MPa nominal yielding strength were adopted in the installation. In the test, four laser displacement sensors (DSs) were placed symmetrically to measure the fixed support plate's sliding displacement, and one laser DS was placed to record the displacement of the loading plate as shown in Fig. 7. The peak displacement Δ_m can be calculated according to the triangle side length relationship. Derived from the literature (Zhai *et al*. 2020), the equation for the peak displacement is $\Delta_m = 0.21D$. which is. Standard cyclic loading protocol was employed to the specimens according to FEMA 461 protocol I (FEMA 461), as shown in Fig. 7. If specimen had not failed in Δ_m, loading cycles with an increment of $0.3\Delta_m$ were continuing to apply until the SSD's failure. The hysteresis curves of the SSDFBs obtained from the test are shown in Fig. 7. The ratios of secondary stiffness to the first yielding stiffness K_2/K_1 for specimen S1 is 2.38, and for specimen S2 is 3.84, respectively. Hence, the SSD was proved to have a large secondary stiffness, which would enhance the structural stiffness under high-level earthquakes, and decrease the residual displacement.

Since the test specimen was symmetry along X direction, half of the SSD was taken out for building a FE model in ABAQUS as shown in Fig. 7. The steel plate and bolt support rod were both modeled by 3D-stress 8-node nonlinear solid element to consider their contact effect. The surface interactions between the bolt hole and support rod were modeled by surface-to-surface contacts with a normal property of hard contact. To model the actually test conditions, the degrees of freedom (DOFs) on the bottom rod end surfaces were all restrained. All DOFs for the top rod end surface were combined to a reference point to which the cyclic displacement protocol was loaded in the X-direction. The established solid model was meshed by 4 elements with 5 mm element size along plate thickness. The material plasticity and geometric nonlinearity were both considered in the numerical model. Owing to there was no obvious plastic deformation of the high strength bolts, elastic material with Young's Modulus 210 GPa and Poisson ratio 0.3 was adopted for the bolt elements. Fig. 8 compares the hysteretic curves of tested specimens and FE models of the SSD. When the displacement is small, the hysteretic behaviors of numerical model agree well with test results. When the displacement is large, the numerical model can accurate simulate the flexural-tensile characteristics and the good energy dissipation capability of the SSD. The forces of numerical models are slightly larger than forces of test specimens, which may be due to the deficiencies and residual stresses in the manufacturing process. Although the numerical models are not precisely considered the fracture and low-cycle fatigue damage and

(a) Specimen 1 (b) Specimen 2

Fig. 8 Accuracy verification of S-shaped plate damper FE model

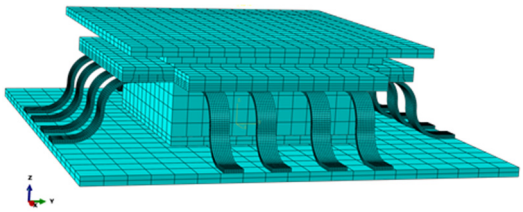

Fig. 9 FE model of the SSDFB

may have an impact on the precision under strong earthquakes of longer duration (Zhai *et al*. 2020). But in summary, the solid numerical model has high accuracy and can be adopted in the numerical study of SSDFB.

3.1.2 FE Model of SSDFB

After verifying the accuracy of the FE model of SSD, the solid FE model of the SSDFB was established in ABAQUS using the same modeling approach. The solid FE model of the SSDFB is shown in Fig. 9. Since there are no obvious plastic deformation of the upper plate, middle plate and bottom plate, their elastic material was adopted for the bolt elements. The element size of the upper plate, middle plate, and bottom plate was set larger than the S-shaped steel plate since they were designed to have much smaller deformations under horizontal load. The AFS and plane slider were simulated utilizing the Coulomb friction relationship with a friction coefficient of 0.1 and a sliding yield displacement of 2 mm (Jiang *et al*. 2019).

3.1.3 Comparison of FE and theoretical Model of SSDFB

For comparing the FE and theoretical model of SSDFB, a type of bearing with 4 SSDs at each side was selected. Fig. 10 shows the deformation contour of the numerical movable SSDFB and the corresponding theoretical curves. When the bearing displacement is within the gap length d_g (15 mm), the bearing is in the normal working stage, at this time only the upper plate appears to slide. As the bearing displacement increases, when exceeds the gap length, the bearing is in the flexural yielding stage, and the additional friction plate and SSD start working together. When the bearing displacement is larger than the second yielding displacement d'_t, the SSD enters the tensile strengthening stage. At this stage, there is an obvious necking phenomenon in tension area of S-shaped steel plates, the stress concentration phenomenon in the place where the bending deformation is also obvious, and the corresponding bearing enters the stiffness strengthening stage. It can be seen that in the process of the one-way cyclic loading of the bearing, only the SSDs in the same direction deformed, and the slide rail on the other side worked to ensure that no out-of-plane deformation in the connected SSDs, which along the changes in the bearing working stages illustrates the accuracy of the established FE model of the SSDFB.

Taking the parameters of the bearings into the Eqs. (10) and (11), the theoretical curves of the SSDFB in the loading process can be obtained. Fig. 11 compares the theoretical and numerical force-displacement relationship of fixed and movable SSDFBs. For both fixed and movable bearings, the

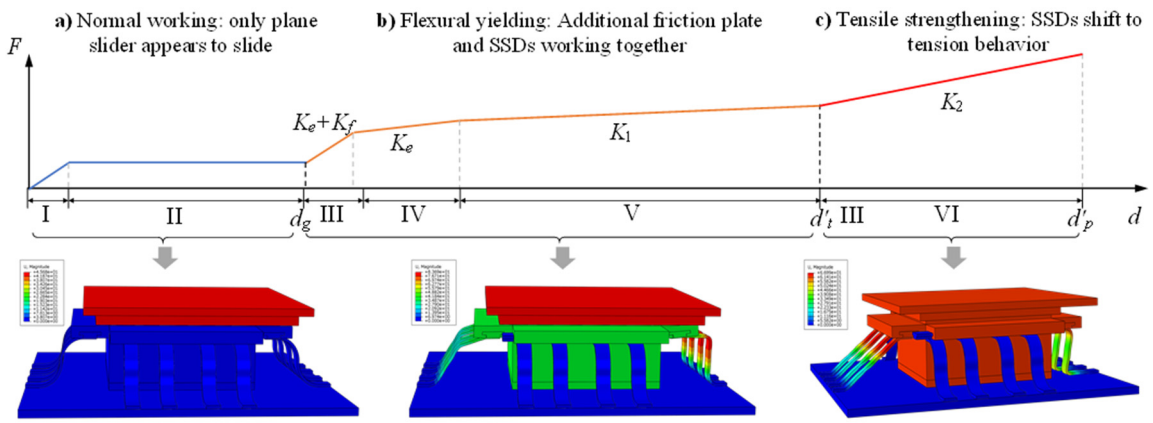

Fig. 10 Correspondence between the displacement contour and the theoretical curves

(a) Fixed bearing (b) Movable bearing

Fig. 11 Force-displacement relationship comparison of SSDFB in the loading process

errors between theoretical and numerical curves in the elastic stage, as well as the flexural yielding stage, are all less than 5%. When the SSDs enter the tensile strengthening stage, the theoretical force is slightly smaller than the FE simulation results. This error mainly comes from the errors in fitting the parameters of the simplified calculation equation for the SSD's force-displacement relationship and assumptions in the derivation. For the fixed bearing, the error percentage is 10.8% at 50 mm. However, the displacement of the fixed bearing under an earthquake with a PGA of 0.57 g does not exceed 30mm, and the corresponding error is 2.85%. Meanwhile, the theoretical formulation is still sufficient to describe the main mechanical properties of SSDFBs, such as K_e, K_1, K_2, K_f, d_g, and d_t, as shown in Fig. 11. The comparison of the FE numerical and theoretical model shows that the theoretical equation can well describe the force-displacement relationship of the SSDFBs, and the FE model is consistent with theoretical analysis which can be used in further parameter studies.

3.2 Parameter studies of the SSDFB

In the practical application of SSDFB, the bridges have different levels of demand on the mechanical properties of the bearings at different seismic intensity zones. Therefore, to guide the application of the SSDFB, the study of the relationship between the mechanical properties and parameters can provide a guide for the selection of parameters in the design. By building FE model of SSDFBs with different parameters, the influences of the dimensions and number of SSDs, the friction coefficient of the AFS and the gap length of the movable SSDFB mechanical characteristics are studied in this section. To ensure the accuracy of the parameter studies of SSDFBs, the vertical force applied to the SSDFB needs to be matched to the practical bearing pressure. Since there are four bearings under each bridge span, the vertical load applied at the bearing FE model is set to be 1/4 of the self-weight (2200 kN) of each bridge span in the normal working stage (Guo *et al*. 2020a).

3.2.1 Influence of dimensions and number of SSDs

The SSDs in SSDFB not only can enhance the energy dissipation capacity of the bearing but also can effectively restrain the large displacement of the girder under strong earthquakes. The influences of SSDs' dimensions and number on the mechanical properties, such as the initial stiffness K_e, yield displacement d_y, yield stiffness K_1, secondary yield displacement d_t, second-order yield stiffness K_2, are investigated here. A constant vertical load was applied to the bearing, and the coefficients of friction of the AFS μ are all taken as 0.1 (Jiang *et al*. 2019). The number of dampers n ranges from 2 to 6. The height of damper D takes the values of 150 mm, 175 mm, and 200 mm. The width b and thickness t of the SSD is 40 mm, 50 mm, 60 mm and 8 mm, 10 mm, 12 mm respectively.

Fig. 12 shows the backbone curves of the SSDFBs with varying SSD dimensions and numbers. From Fig. 12(a), it can be seen that the initial stiffness, yield force and the yielding stiffness of the bearing increase with the increase in the number of SSDs, and the energy dissipation capacity and ultimate bearing capacity also increase. On the other side, increasing the number of dampers, which also increases the initial stiffness, requires more force to yield for the steel plate and appear to dissipate energy through flexural plastic deformation. From Fig. 12(b), it can be seen that the height D of the SSD has no significant effect on the initial stiffness, sliding yield force and ultimate bearing capacity, but is positively related to the bearing's

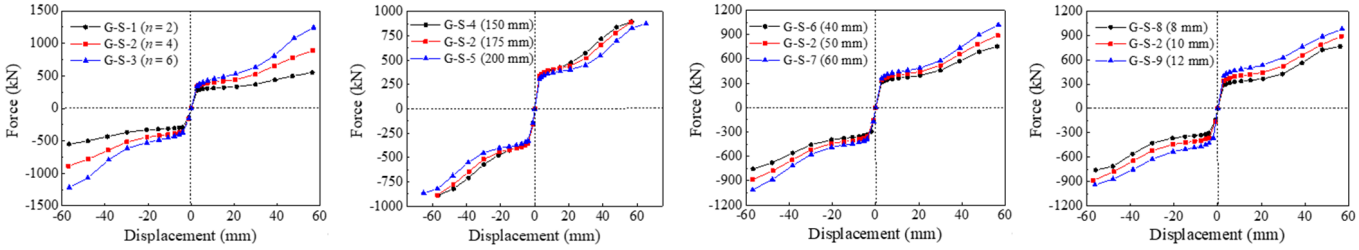

(a) n (b) D (c) b (d) t

Fig. 12 Influence of SSD parameters on backbone curves

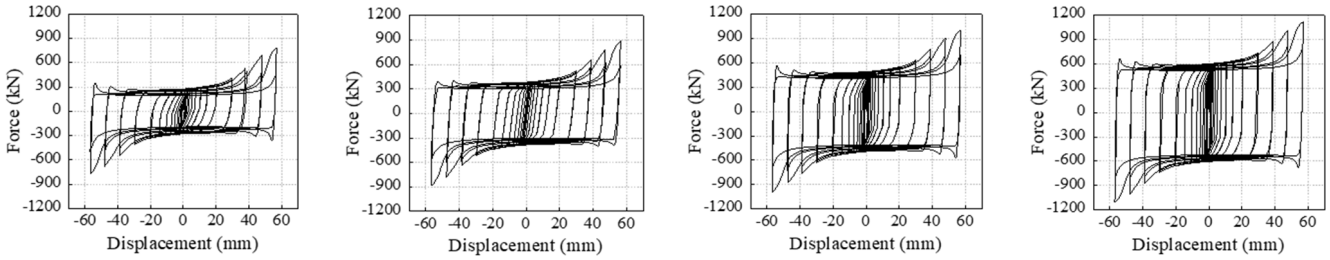

(a) G-M-1 (μ = 0.05) (b) G-M-2 (μ = 0.1) (c) G-M-3 (μ = 0.15) (d) G-M-4 (μ = 0.20)

Fig. 13 Hysteresis curves with varying friction factors

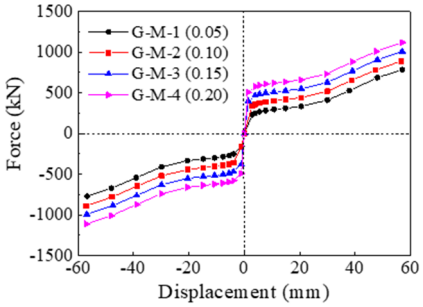

Fig. 14 Backbone curves with different friction coefficient

deformation capacity. In the case of equal horizontal force, the higher the height D, the greater the deformation of the bearing, and the K_1 of the bearing becomes smaller with increasing D. As shown in Figs. 12(c)-(d), the width and thickness of the S-shaped steel plate are both positively correlated with initial stiffness, SSD yield force, K_1 and K_2, because both of these factors increase the steel plate's cross-sectional area.

3.2.2 Influence of the friction coefficient

The friction of AFS is another major energy dissipation mechanism of the SSDFB. The varying friction coefficient changes the mechanical properties and energy dissipation capacity of the bearing. Based on the fixed bearing, the effect of different friction coefficients on the mechanical properties of the SSDFB was analyzed, while keeping the vertical load N and SSD parameters constants, where N = 2200 kN, n = 4, D = 175 mm, b = 50 mm, and t =10 mm. The friction coefficients μ of four SSDFB specimens are ranging from 0.05 to 0.2 (Ozbulut and Hurlebaus 2011).

Fig. 13 shows the hysteresis curves of SSDFBs with different μ. Fig. 14 shows the corresponding backbone curves. The hysteresis loop area increases as the μ increases. In turn, the energy dissipation capacity of the bearing is enhanced. On the other hand, the results show that the larger μ is, the larger initial stiffness, slide yielding force and ultimate bearing capacity is. Under the same loading displacement, the horizontal force of the bearing increases with the increase of μ, but stiffness of the bearing after yielding and sliding are not affected because the second segment of the Coulomb friction model is a constant value. It is worth noting that although increasing μ of the AFS can improve the energy dissipation capacity and ultimate bearing capacity of the bearing, but the sliding yield force is also significantly increased. Under the earthquake of different intensities, a reasonable value of μ is required to effectively perform the isolation and seismic dissipation functions.

3.2.3 Influence of the gap length

To release the deformation and internal force caused by the temperature change, a gap is reserved in the movable bearing, which also influences the hysteresis characteristics of the bearing. Here four SSDFB with different gap length d_g (15 mm, 25 mm, 35 mm, and 45 mm) is selected while keeping other parameters equal, where N = 2200 kN, n = 4, D = 175 mm, b = 50 mm, t =10 mm, and μ = 0.1. Mechanistically, the gap in movable bearing causes a delay in the functioning of the AFS and SSDs. Fig. 15 shows the hysteresis curves with different gap lengths of SSDFB under standard cyclic loading, and Fig. 16 shows the backbone curves of SSDFB. It is shown that there is a lag in the hysteresis energy consumption. The results also show that the larger the gap length d_g is, the larger delay of the AFS and SSDs start working is. When the displacement of the bearing is greater than the gap length, AFS and SSDs begin to function, AFS begins to slide, SSD deforms, then

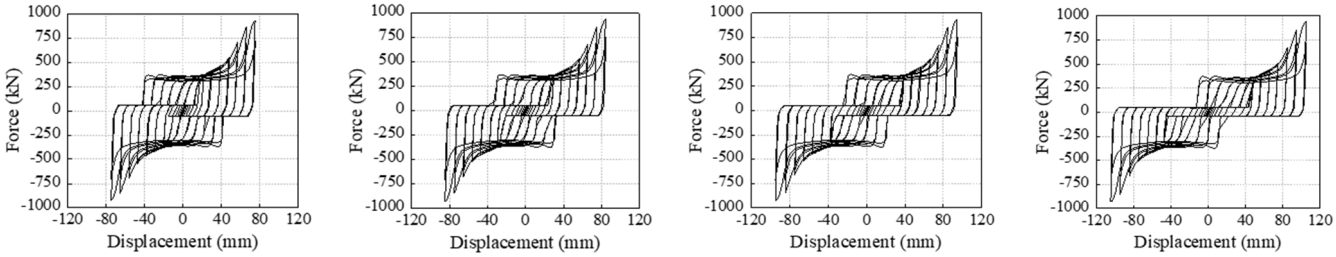

(a) H-D-1 (d_g = 15 mm) (b) H-D-2 (d_g = 25 mm) (c) H-D-3 (d_g = 35 mm) (d) H-D-4 (d_g = 45 mm)

Fig. 15 Hysteresis curves with varying gap length

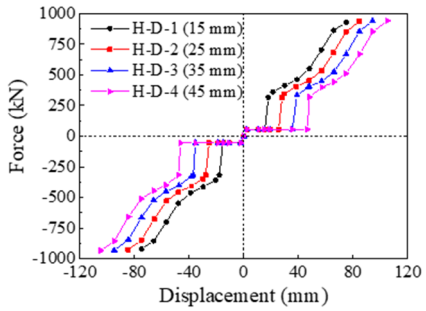

Fig. 16 Backbone curves with different gap length

movable bearing performs the function of seismic dissipation. The hysteresis results show that the K_1 and K_2 is not affected by the gap length.

4. Model of CRTS-II simply supported bridges and ground motion selection

4.1 Prototype bridges

The typical five-span HSR SSB was chosen for this study (Guo *et al*. 2021), as shown in Fig. 17. This bridge adopts the standard span of China's HSR SSBs, with a length of 32.6 m and a girder gap of 0.1 m. Considering the transition section of subgrade and bridge, unequal pier height, and upper track structure. The box girder and round-ended pier are made of reinforcement concrete. The girders numbered B1–B5 from right to left, which are longitudinally fixed at one end and are horizontally fixed at both ends. The five-span bridge takes the subgrade-bridge transition as a boundary, which consists of a 50-m long friction plate. The CRTS-II slab ballastless track structure (He *et al*. 2017) is mounted on the girder as shown in Fig. 17, in which the base plate, track plate, and steel rail are all longitudinally continuous. The supporting parts of the bridge are numbered sequentially, with two abutments numbered as A0 and A5, and with piers numbered P1–P4 from right to left. The height of P1 and P4 is 8 m and the height of P2 and P3 is 16 m. The arrangement of the different types of bearing at the pier top is also shown in Fig. 17. The dashed arrow on the bearing indicates the movable direction of the bearing, without an arrow means it is fixed in that direction.

4.2 Numerical model

4.2.1 Numerical model of bridge-track structure

The cross-section of the piers in Fig. 17 indicates the weak resistance of the HSR SSB in the longitudinal direction and suggests that damage is likely to occur under a longitudinal earthquake input (Jiang *et al*. 2019). Therefore, a two-dimensional numerical model of a HSR bridge was established in OpenSees. The longitudinal seismic analysis was performed while ignoring the vertical earthquakes (TB 10621-2014, Li *et al*. 2021). The nonlinear FE model of the bridge–track structure in OpenSees is shown in Fig. 18. The shear grooves and shear bars locate near the fixed bearing, connecting the base plate with girder and the track plate with the base plate, respectively. The connect components such as the fasteners, mortar layer, sliding layer, embankment, end spines, bearings, shear grooves and shear bars were modeled by zero-length element considering their non-linear behaviors (Guo *et al*. 2020a); the longitudinal element such as rail, track plate, base plate and girders are modeled using elastic beam-column element, the parameters of girder and track components are listed in Table 1 (Zhai and Xia 2001). The fasteners that connect steel rail and track plate was simulated with a spacing of 0.65 m between two elements. The TwoNodeLink element was used to model the pier, and the pier bottom was fixed to the ground. The mass of the bridge modeled by the concentrated mass method, in which the mass is concentrated on the element node. The force-displacement curves of the 8-m and 16-m piers were obtained using a cyclic loading test by Shao *et al*. (2014), which was modeled using Pinch-4 material.

4.2.2 Numerical model of SSDFB in OpenSees

The commonly used spherical bearing was modeled by the nonlinear zero-length element, whose displacement-force relationship is shown in Fig. 19. The ideal elasto-

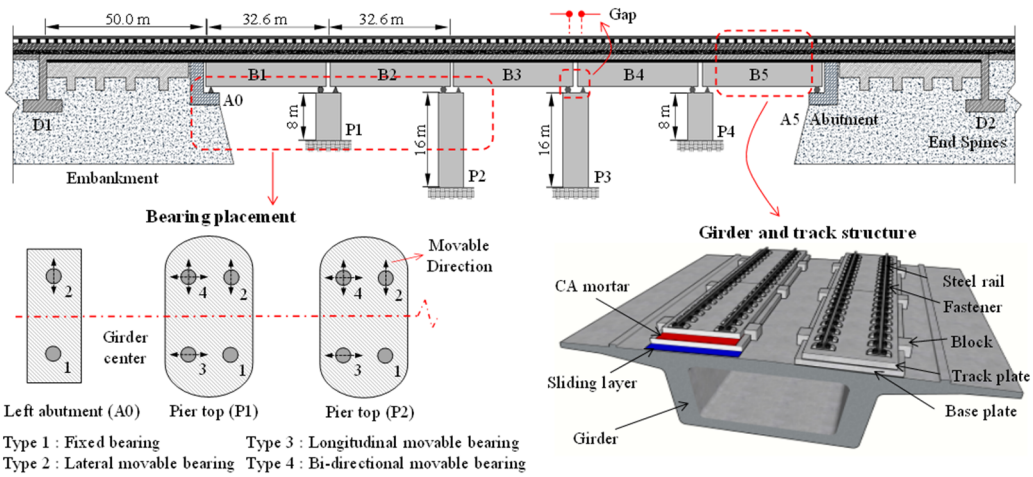

Fig. 17 Typical five-span high-speed railway simply supported bridges

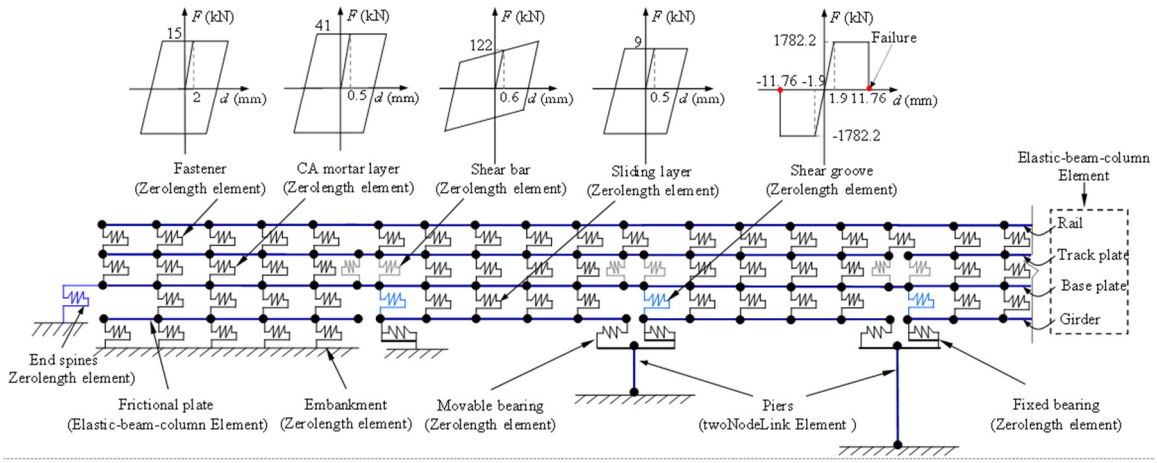

Fig. 18 Finite element model of HSR bridge in OpenSees (1/2 model)

Table 1 Parameters of girder and track components

Components	Strength	Area	Elastic modulus	Moment of inertia
Girder	23.1 MPa	8.34×10^5 mm^2	4.40×10^4 N/mm^4	9.00×10^{12} mm^4
Base plate	14.3 MPa	3.60×10^6 mm^2	3.0×10^4 N/mm^4	4.80×10^{12} mm^4
Friction plate	14.3 MPa	5.10×10^5 mm^2	3.60×10^4 N/mm^4	1.70×10^{12} mm^4
Track plate	23.1 MPa	5.60×10^5 mm^2	3.25×10^4 N/mm^4	1.68×10^{12} mm^4
Rail	500 MPa	7.75×10^3 mm^2	2.06×10^5 N/mm^4	0.32×10^2 mm^4

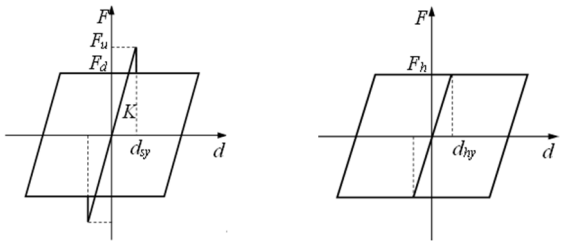

(a) Fixed bearing (b) Movable bearing

Fig. 19 Normal Railway spherical bearing displacement-force relationship

plastic bilinear material was adopted for modeling the movable bearing and the friction stage of fixed bearing after the shear key breaks (Kang *et al*. 2017). Meanwhile, for the fixed bearing, the MinMax material was combined with the elastoplastic bilinear material for modeling the shear key normal working and damage phase.

In section 3, the solid FE model of the SSDFB was built in ABAQUS, and the accuracy of the numerical model was verified by comparing it with the experimental and theoretical results. To study the seismic reduction effect of the proposed SSDFB, the numerical model of SSDFB was model in OpenSees by combining different types of macro-elements and calibrated against solid FE model. Fig. 20 shows the modeling approach of movable and fixed SSDFB in OpenSees. For the movable bearing, the gap, plane slider, S-shaped steel damper and additional sliding surface component are modelled by gap element, plane slider bearing element, zero-length element and plane slider bearing element, respectively. The gap and plane slider were connected in series and connected in series with the parallel system formed by an S-shaped steel damper and an additional sliding surface. The fixed bearing FE model includes an S-shaped steel damper, shear key, and additional sliding surface components, the three are connected in parallel and simulated by zero-length

(a) Movable bearing (b) Fixed bearing

Fig. 20 Numerical model of SSDFB in OpenSees

(a) Movable bearing (b) Fixed bearing

Fig. 21 Comparison of hysteresis curves of SSDFB in OpenSees and ABAQUS

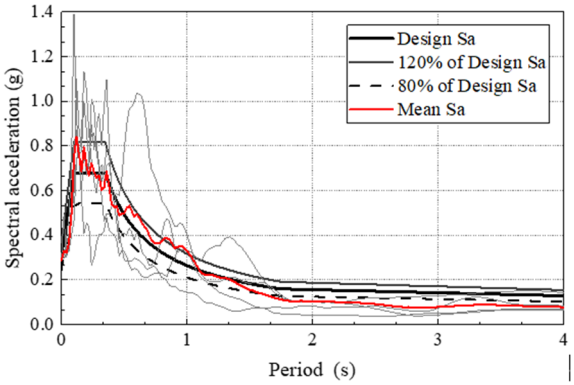

Fig. 22 Comparison of design spectrum with selected earthquakes response spectrum

elements, MinMax element, and plane slider bearing element, respectively. Since the vertical earthquake was not considered, the vertical force applied to the SSDFB in OpenSees is the self-weight of the bridge, which is equivalent to the vertical force of the FE model in ABAQUS. Comparison of hysteresis curves of SSDFB modelled in OpenSees and ABAQUS are shown in Fig. 21. The results are in good agreement under same vertical load, which verifies the accuracy of the OpenSees FE model of SSDFB and can be used in seismic control analysis.

4.3 Selection of ground motions

The seismic fortification intensity of the site is 8 degrees according to China's railway seismic code (Kang *et al*. 2017), and the site type is class 2. According to the code, the PGA of the design earthquake is 0.3 g, the HSR bridge has good seismic performance at this intensity and will not be significantly damaged (Guo *et al*. 2020c). Therefore, the seismic reduction effects of SSDFB were analyzed at high-level earthquakes, and the PGA was adjusted to 0.57 g. Five ground motion records were selected from the Pacific Earthquake Engineering Research Center (PEER) database, as listed in Table 2. The comparison of the acceleration response spectrum (S_a) of the selected ground motion records with the design S_a is shown in Fig. 22, which shows that the error between the mean S_a and the design S_a is less than 20% in the concerned period range, so the selected records meet the criteria of the code.

5. Application performance of the SSDFB

5.1 Analyze cases

In sections 2 and 3, the composition and working principle of the SSDFB were described, the theoretical model was derived, and the influence of each parameter of the bearing on its hysteresis characteristics is studied. In this section, the SSDFBs were applied to the standard five-span HSR bridges. Then, conduct nonlinear dynamic time analysis and compare with normal bearings to investigate the isolation performance of SSDFBs. Three analyze cases with the same arrangement are considered here:

Isolated Case 1: Spherical bearing (SB). The friction spherical bearings were adopted in the HSR bridges. The standard railway spherical bearing displacement-force relationship is shown in Fig. 19, and the type of bearing was chosen as TJQZ-5000 (TB 10621 2014). For the fixed SB, when the shear key breaks, the bearing turned into friction slide and enters the isolation state.

Isolated Case 2: SSDFB. In order to improve the seismic performance, SSDFBs are introduced in the HSR bridge-track structure to replace conventional SB in isolated case 1 between bridge superstructure and substructure. The arrangement of the SSDFBs is the same as isolated case 1.

Non-isolated Case: The SSBs based on the SB in

Table 2 Selection of ground motions

Seismic records	Name	Station	Magnitude	Year
G1	Imperial Valley-02	El Centro Array #9	6.95	1940
G2	Northridge-01	FAI095	6.69	1994
G3	Borrego	El Centro Array #9	6.5	1942
G4	San Fernando	LA-Hollywood Stor FF	6.61	1971
G5	Southern Calif	San Luis Obispo	6	1952

isolated case 1, was adopted here as a comparison. The shear key of SSB is reinforced, and it is assumed that its fixed bearing will not damage under earthquake and therefore will not show seismic isolation effect.

5.2 Definition of damage states and response decrease ratio

To clarify the pier's damage status, the yield displacement d_y and yield force F_y should be defined at first. The Park method (Park 1988) or $0.75F_{max}$ method was adopted here for calculating pier's yield force. The index of response reduction ratio η is defined here for evaluating the SSDFB's effect. The definition of η is the difference of R_0 and R to R_0 ratio, which is given as Eq. (12).

$$\eta = (R_0 - R)/R_0 \times 100\% \tag{12}$$

where, R represents the peak response of bridge-track structure in case 2, i.e.: the SSDFB isolated case; R_0 represents the peak response of bridge-track structure in cases that SSDFB didn't adopted in bridges. The larger η is, the better the isolation effect of SSDFB.

5.3 Performance targets and design of SSDFB

To ensure the safety of the HSR bridges during an earthquake and the resilience after an earthquake, the "code for seismic design of railway engineering" (GB 50111-2006) in China proposes three seismic performance targets. The specific expressions are shown below, and the corresponding requirements of the proposed SSDFB are also explained as an extension of the code.

1) *Target I*: Under low-level earthquakes, the HSR bridge should still maintain normal operations, and the bridge structure overall is in an elastic working condition. The seismic isolation bearing, under low-level earthquakes, should not perform the isolate function, and the shear keys in isolation bearings should keep in the un-sheared state.
2) *Target II*: Under design earthquakes, possible damages may occur to the bridge, and the entrance to inelastic stages of structural components is allowed, but the damages should still be within the repairable range. Through fast and economical repairs, the normal operation of high-speed trains should be resumed. The fixed bearing at the abutment is subjected to a large shear force under earthquakes because the stiffness of abutment is very high (Guo *et al*. 2020c). Therefore, to avoid the fixed bearing damage under low-level earthquakes, the bearing capacity of the support needs to be increased accordingly. But the higher the bearing strength is, the larger the abutment shear force is, which may lead to severe abutment damages that don't meet the resilience requirements. The fixed bearing at the abutment is set to function as an isolator before the seismic intensity reaches the design earthquake, which could decrease the structural seismic response since the SSDFB bearing is very easy to repair, which could be repaired very fast.
3) *Target III*: Under high-level earthquakes, the structure may suffer serious damages: piers will enter the yield state, the girders will have large displacements and the possibility of collision. The track structure also will have different degrees of damage. But the damage still needs to be controlled within a reasonable range and the structure should not collapse. Therefore, under high-level earthquakes, all fixed and movable SSDFB should be designed to enter the isolation stage, performing seismic isolation capability and reducing overall structural responses.

In this study, the design of SSDFB was based on the iterative design method, which is shown in Table 3. At first, the bearing parameters were pre-defined based on normal usage requirement. The friction coefficient μ_p of plane slider referring to the spherical bearing was taken as 0.03. Under the temperature difference of 40℃, the longitudinal deformation of the beam is 13 mm, according to which the movable bearing gap distance d_g is set to 15 mm. Based on the single pier model (Guo *et al*. 2020b), then the bearing reaction force F_r at each pier is roughly determined by the response spectrum method. In turn, other parameters shear key max shear force F_s, friction coefficient of additional surface μ, S-shaped steel plate number n, S-shaped steel plate dimensions D, b, and t of the bearings are initially set. Subsequently, the seismic non-linear dynamic analysis of

Table 3 Design algorithm for SSDFB

Algorithm 1 Design algorithm for SSDFB

Input: Bridge paramaters; seismic fortification intensity of the site

Output: Parameters of SSDFB: $F_s, n, D, b, t, \mu, \mu_p, d_g$

initialize: Set μ_p and d_g
initialize: Set F_s, n, D, b, t, μ
Chose groud motions and adjust PGA to different levels
Time history analysis
Obtain F_{max}, D_{max} and F_r
while (F_{max} and F_r meet the target) or ($D_{max} > D_{lim}$) **do**
    Modify SSDFB parameters: F_s, n, D, b, t, μ
    Time history analysis
end while

Table 4 Parameters of designed SSDFB

Bearing number	F_s (kN)	d_g (mm)	n	D (mm)	b (mm)	t (mm)	μ	μ_p
GXZ1, GXZ3, GXZ4	1500	/	15	175	50	10	0.25	0.03
GXZ2, GXZ5	1000	/	6	175	50	10	0.1	0.03
HXZ1, HXZ3, HXZ5	/	15	6	175	50	10	0.1	0.03
HX/2, HXZ4	/	15	15	175	50	10	0.25	0.03

the isolated bridge under different level earthquakes are performed to evaluate whether the results meet the three-stage design target, taken the peak pier bottom force F_{max} and peak girder displacement D_{max} as indicators. If the indexes don't meet the requirement, return to the parameter's selection process for iterative calculation.

Based on seismic fortification intensity of the site, the PGA of the low-level, design, and high-level earthquakes for the three stages of design target are 0.10 g, 0.30 g, and 0.57 g, respectively. One group of designed bearing parameters that meets the target are shown in Table 4. In the table, the fixed bearing from left to right are numbered from GXZ1 to GXZ5, and the movable bearing from left to right are numbered from HXZ1 to HXZ5. However, due to the many parameters of the SSDFB, the iterative design method used in this study is still preliminary and requires a larger iterative computational effort. The parameters may not be the optimal solution and the seismic control performance of the SSDFBs can be further improved since limited iteration were conducted and ground motions were selected in this study.

5.4 Seismic control effects on bridge structure

5.4.1 Bearings

Fig. 23 shows the hysteresis loop of fixed and movable SSDFB under earthquake G1. The results show that under high-level earthquakes the shear key of fixed bearings were all sheared off, and the S-shaped steel plates of fixed bearings were entered the flexural yielding stage and started energy dissipation. Besides, there was a significant stiffness increase (the second stiffness K_2) in fixed bearing caused by the tensioning behavior of the S-shaped steel plate at large displacement, as shown in Fig. 23(a). For the movable bearings, as shown in Figs. 23(b)-(d), the bearing displacements were all exceeded the gap length and started energy dissipation by friction combining with steel flexural yielding together. In summary, the SSDFB's hysteresis curves are full and have strong energy dissipation capability, which basically achieves the target of seismic design.

The large displacement of movable bearing may cause bridge unseating or even girder collision damages. To clearly analyze the displacement response of different isolation cases under high-level earthquakes, Fig. 24

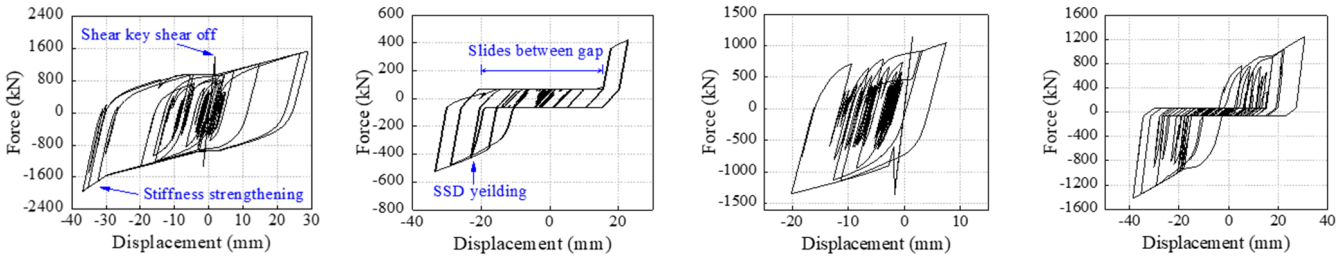

(a) Fixed bearing GXZ3 (b) Movable bearing HXZ3 (c) Fixed bearing GXZ4 (d) Movable bearing HXZ4

Fig. 23 Hysteresis loop of SSDFB under earthquake G1

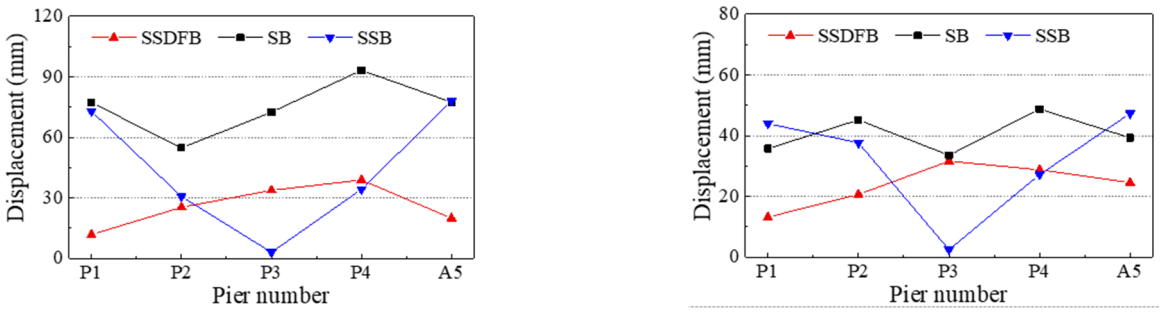

(a) Displacement under earthquake G1 (b) Displacement under earthquake G2

Fig. 24 Peak displacement responses of movable bearing

Table 5 Peak displacement responses and η of movable bearing under earthquakes

Records	Cases	Bearing position							
		P1		P2		P3		P4	
		Displacement (mm)	η	Displacement (mm)	η	Displacement (mm)	η	Displacement (mm)	η
G1	SSDFB	11.78	/	25.36	/	33.74	/	38.87	/
	SB	77.26	84.76%	54.75	53.67%	72.52	53.47%	93.23	58.31%
	SSB	72.90	83.84%	30.64	17.24%	3.02	-1018.1%	34.24	-13.51%
G2	SSDFB	13.16	/	20.67	/	31.62	/	28.75	/
	SB	35.72	63.15%	45.22	54.28%	33.56	5.78%	48.76	41.04%
	SSB	43.97	70.06%	37.66	45.10%	2.46	-1187.8%	27.15	-5.89%
G3	SSDFB	13.85	/	17.95	/	22.93	/	30.00	/
	SB	62.23	77.74%	26.84	33.12%	2.18	-950.4%	31.20	3.83%
	SSB	33.51	58.66%	26.16	31.38%	2.10	-993.3%	21.37	-40.36%
G4	SSDFB	7.67	/	24.77	/	28.05	/	26.53	/
	SB	6.74	-13.74%	42.77	42.09%	1.63	-1623.6%	43.02	38.32%
	SSB	41.35	81.45%	37.76	34.41%	2.94	-854.9%	36.07	26.44%
G5	SSDFB	7.19	/	30.84	/	35.50	/	38.60	/
	SB	4.77	-50.66%	76.62	59.75%	40.32	11.95%	76.38	49.46%
	SSB	13.42	46.41%	102.76	69.99%	3.54	-902.5%	108.63	64.47%

compares the movable bearings peak displacement response of different piers under earthquakes G1 and G2, which is the relative displacement of the girders and piers. Table 5 lists the peak displacement responses and response reduction ratio η of movable bearing under selected earthquakes. The results show that the bearing peak displacements from P1 to P5 of SSDFB are all significantly smaller compared with SB; the SSDFB's peak displacements are overall reduced compared with SSB, which shows that the SSDFB enhanced energy dissipation capacity of HSR bridge-track structure and the relative displacements of the girders and piers are limited. It is proved that the SSDFB can effectively restrain the displacement of the girder and prevent the occurrence of bridge unseating.

But under same the earthquake, the SSB peak displacement at P3 is obviously smaller than that of SB and SSB, which induced the η of SSDFB at P3 to be a negative value. The reason is that when the normal SBs were strengthened to ensure the fixed bearings would not damage under earthquakes, the investigated five-span bridges are a symmetry structure since the height and stiffness of P2 are similar to P3. Thus, there were approximate consistent deformations of pier P2 and P2, which would induce very small or even close to zero displacements of movable bearing at P3. But in the case of SSDFBs, the fixed and movable bearings are all function as isolation and energy dissipation devices, and there was a relative displacement between pier P2 and P3, which would produce a larger displacement of SSDFB movable bearing than the SSB. However, it is also because of the relative motion, the new bearing can dissipate a larger amount of seismic energy, thus achieving the purpose of reducing the overall response and protecting the structure.

5.4.2 Piers

Fig. 25 compares the pier-top displacement responses of different isolation cases under earthquake G1. Compared with the SB and SSB cases, the result shows that the displacement responses of different piers are largely reduced when the SSDFBs were adopted, especially for the pier P1 and P4, which verified that the SSDFB has a good seismic control effect on pier displacement responses. Due to the isolation and energy dissipation effect of SSDFB, the peak displacement of each pier was below the corresponding yield displacement, while the peak pier displacement in the cases that adopted SB and SSB were all exceeded the yield limit. From Fig. 25 we can also see that the residual displacements of 8-m pier P1 and P4 were largely reduced by the SSDFBs, which was beneficial to the rapid restoration of bridges for operation after a major earthquake. The pier bottom shear force responses of three different cases under earthquakes G1 and G2 are shown in Fig. 26, and the results clearly show that the shear force of piers was effectively reduced when the SSDFB was adopted, compared with the SB and SSB cases. This is due to the period enlarge effect of the seismic isolation bearing. In addition, SSDFB has a combination of energy dissipation capability, and the earthquake energy input to the bridge structure can be effectively dissipated. On the other hand, after the SB was strengthened, the shear force of piers was also increased, because SSBs did not yield for energy dissipation and the forces transferred from superstructure to the piers were therefore increased.

Table 6 lists the different pier's peak displacement response and response reduction percentage η of SSDFB under earthquakes of three isolation cases. Under ground motion G1, compared with the bridge with SB, the η of 8-m pier P1 is 75.5% and the η of 16-m pier P2 is 47.3%;

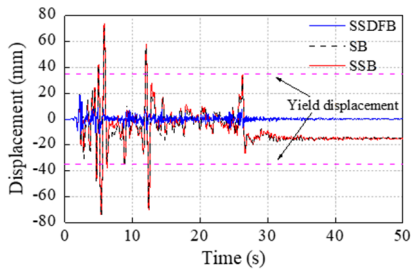

(a) P1

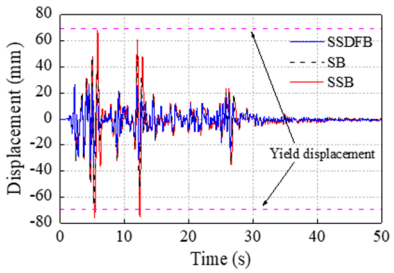

(b) P2

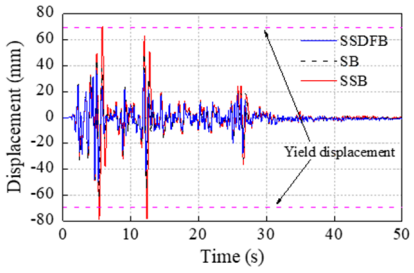

(c) P3

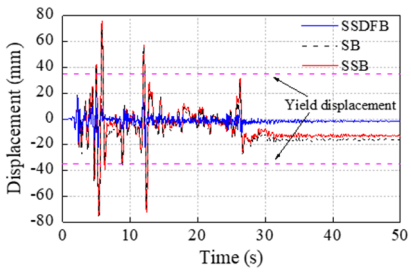

(d) P4

Fig. 25 Pier-top displacement responses under earthquake (G1)

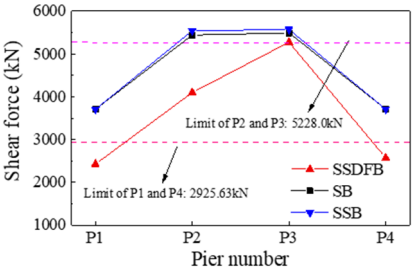

(a) G1

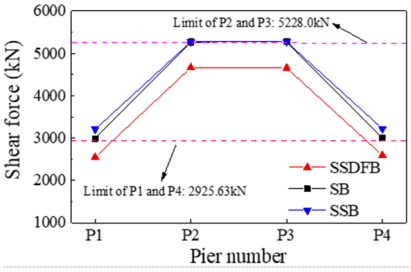

(b) G2

Fig. 26 Pier bottom shear force responses under earthquakes

Table 6 Peak pier displacement and η under earthquakes

Records	Cases	P1		P2		P3		P4	
		Displacement (mm)	η	Displacement (mm)	η	Displacement (mm)	η	Displacement (mm)	η
G1	SSDFB	18.44	/	34.56	/	49.10	/	22.26	/
	SB	75.16	75.5%	65.59	47.3%	70.59	30.4%	77.01	71.1%
	SSB	74.28	75.2%	75.81	54.4%	78.47	37.4%	76.12	70.8%
G2	SSDFB	21.54	/	38.86	/	41.72	/	22.78	/
	SB	37.22	42.1%	48.05	19.1%	48.88	14.7%	37.80	39.7%
	SSB	45.34	52.5%	48.58	20.0%	48.53	14.0%	45.92	50.4%
G3	SSDFB	23.47	/	41.52	/	40.14	/	25.39	/
	SB	33.46	29.9%	42.67	2.7%	43.26	7.2%	34.50	26.4%
	SSB	30.13	22.1%	50.37	17.6%	50.79	21.0%	35.90	29.3%
G4	SSDFB	19.94	/	31.16	/	39.05	/	17.43	/
	SB	19.47	-2.4%	44.67	30.2%	46.01	15.1%	18.65	6.5%
	SSB	41.22	51.6%	44.44	29.9%	45.04	13.3%	43.21	59.7%
G5	SSDFB	19.71	/	34.38	/	52.00	/	24.57	/
	SB	20.28	2.8%	72.00	52.3%	71.55	27.3%	18.66	-31.7%
	SSB	16.13	-22.2%	92.96	63.0%	96.73	46.2%	17.07	-44.0%

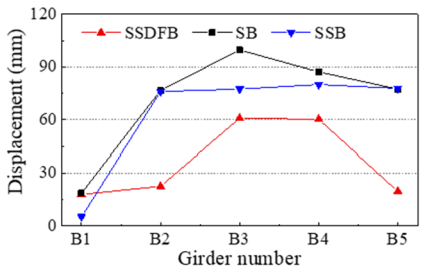

(a) Girder displacement under earthquake G1

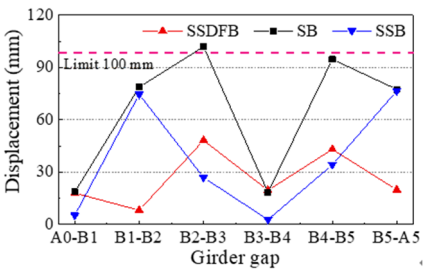

(b) Girder gap under earthquake G1

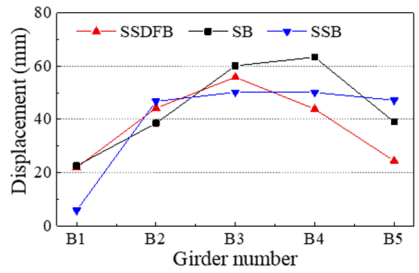

(c) Girder displacement under earthquake G2

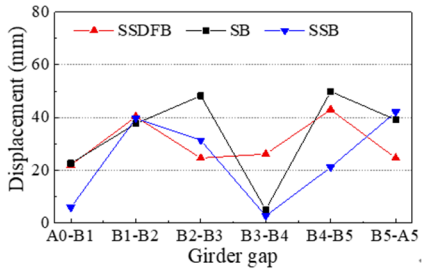

(d) Girder gap under earthquake G2

Fig. 27 Peak girder displacement and girder gap under earthquakes

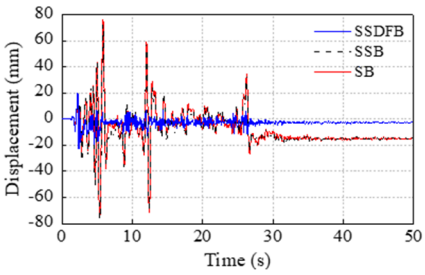

(a) Girder B2

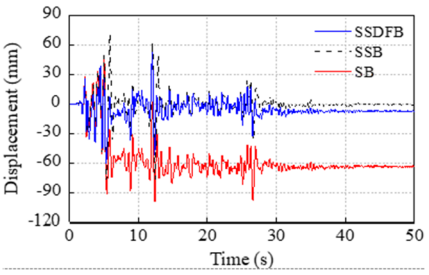

(b) Girder B3

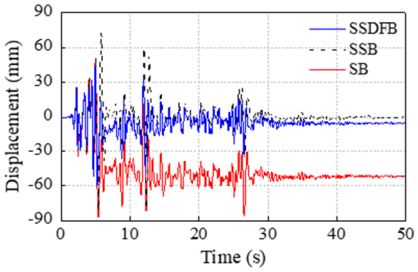

(c) Girder B4

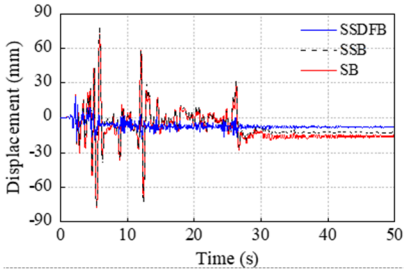

(d) Girder B5

Fig. 28 Longitudinal displacement of girders under earthquake (G1)

compared with the bridge with SSB, the η of 8-m pier P1 is 75.2% and the η of 16-m pier P2 is 54.4%, which proves that the SSDFB has significant reduction effect on pier displacement. Though strengthening the SB can reduce the possibility of bearing damages, but the SSB cannot reduce the pier responses, sometimes even largely increases the responses, which is unfavorable in terms of structural recoverability. In summary, the SSDFB significantly reduced the pier responses under earthquakes, delayed the time for the pier to enter the yielding stage, ensuring that the pier can remain in an elastic working condition under higher earthquake intensities.

5.4.3 Girders

Due to the longitudinal track structure that mounted on HSR bridges, the constrain condition of the girders in HSR bridge-track structure is very different of constrain condition in highway bridges, which is only restrained by bearings on piers and has no other constraints. Therefore, there were much more complex forces and multiple interactions on the HSR girders when the bridges were subjected to earthquakes. Fig. 27 shows the comparison of peak girder displacement and girder gap responses under earthquakes for the different isolation cases. The results show that the SSDFB can effectively reduce the peak girder displacements and the girder gap changes overall, and the

control effects of the SSDFB are larger when the girder displacement is larger. For instance, under earthquake G2 the peak girder displacement was reduced from 63.35 mm to 55.84 mm; but under earthquake G1 the peak girder displacement was reduced from 99.61 mm to 60.88 mm since there were more energy dissipation at large displacements and greater strengthening stiffness of SSDFB. The reduction of girder gap changes prevents the failure of girder collision. Under earthquake G1, the peak girder gap changes of B2 and B3 was 101.85 mm, which was larger than the max girder distance of 100 mm, therefore a collision cooccurred. After adopting SSDFB, the relative displacement was reduced to 48.21 mm, and the η reaches 52.7%, which significantly reduces the possibility of girder collision, because the SSDFB played the function of restrainer when the relative displacement is large. Though the SSB also has good control effects on girder displacement but has a very adverse cost to the bridge pier, shown in the last section.

It is noteworthy that, while evaluating the seismic control effect of isolation bearings, the residual displacement of bridges is also an important index besides the structure peak responses. Fig. 28 shows the longitudinal displacement of girders under earthquake G1. It can be clearly seen that the SSDFB significantly reduced the residual deformation of the girders. Because the large secondary stiffness of the SSD provides sufficient restraining force for the girders and enhances the structural strength and stiffness at high seismic demand. This will reduce the repair time and cost of HSR bridges after the earthquake and ensure the rapid resumption of operations.

5.5 Seismic performance of SSDFB on track structure

The CRTS II track structure is built on HSR bridges, which is a longitudinal continuous structure with multiple layers of force transmission elements. One of the reasons for the absence of isolation bearings in HSR is concerned about the harm on track structures of isolation bearings. To study the seismic performance of SSDFB on track structure, in this section, the seismic responses of the connection components and the longitudinal continuous components of track structure are investigated in different isolation cases.

5.5.1 Connection components of track structure

The sliding layer locates between the base plate and girders, which ensures these two components move freely under temperature load. As shown in section 5.4, the peak girder displacement responses are limited while the SSDFB was adopted, which would certainly affect the seismic responses of sliding layer. Figs. 29(a)-(b) compares the peak displacement responses of sliding layer under earthquakes. The results show that the peak displacement of the sliding

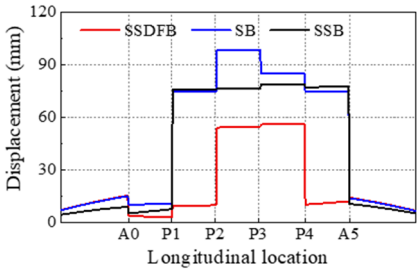

(a) Sliding layer under earthquake G1

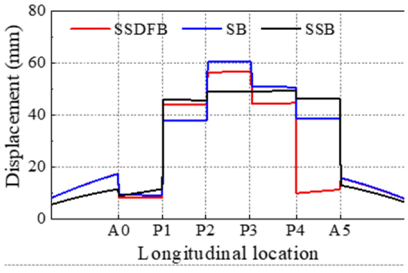

(b) Sliding layer under earthquake G2

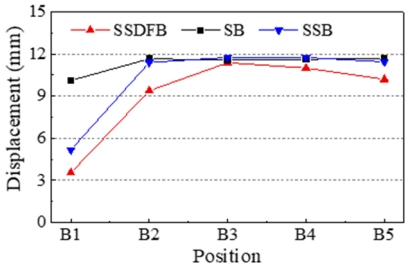

(c) Shear groove under earthquake G1

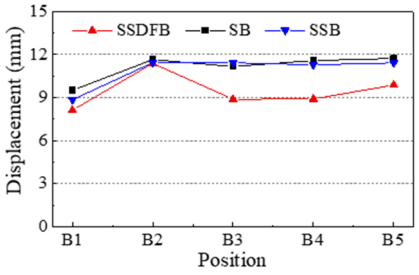

(d) Shear groove under earthquake G2

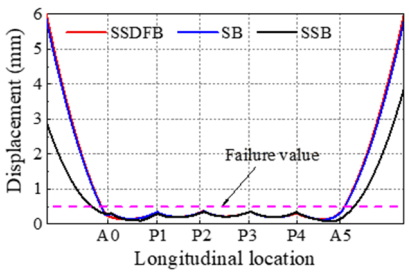

(e) CA mortar layer under earthquake G1

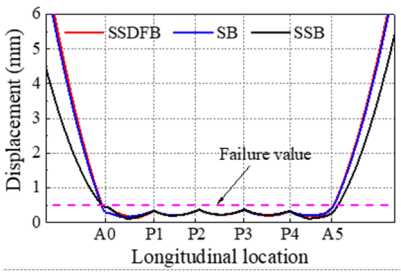

(f) CA mortar layer under earthquake G2

Fig. 29 Peak displacement of filling and connecting components under earthquakes

layer has been reduced to some degree by adopting the SSDFB. Under earthquake G1, the sliding layer's peak displacement while SSDFBs were adopted was reduced by 42.36 mm, and the response reduction ratio was 75.64%. Similar to the sliding layer, the shear groove is the connecting component between base-plate and girders, transferring forces from the track structure to the bridge. The responses of the shear groove are mainly determined by the relative displacement between the base plate and girders. Figs. 29(c)-(d) shows the peak displacement of shear grooves under earthquakes. It can be seen that the groove displacements were reduced from B1 to B5 when the SSDFB was adopted, since the SSDFB largely reduced girders' displacement compared with SB and SSB. Figs. 29(e)-(f) gives the peak displacement responses of CA mortar layer in different isolation cases, which shows that the CA mortar layer's seismic response pattern was similar to different isolation cases. The displacement of the mortar layer above girders are small, which didn't exceed the limit shear displacement (0.5 mm) and is not sensitive to the bearing type. But the peak displacement of the mortar layer of three cases above the embankment were all larger than the limit value where SSB was the minimum.

5.5.2 Longitudinal continuous components

Figs. 30(a) and (b) compare the peak stress of base-plate of different isolation cases under earthquakes. The results show that there is a similar change pattern and magnitude of three cases, in which the max stress increases gradually from the middle of the bridge to the embankment, and the stress reaches the peak value at the position of end spines. When the SSB was adopted, the max stress was slightly smaller above the embankment, which was because the SSB strengthened the connection between girder and abutment. Max stress of the track plate under earthquakes is shown in Figs. 30(c)-(d), and the max stress of the rail is shown in Figs. 30(e)-(f). The peak stress distribution of track plate and rail are similar: the peak stress value occurred in abutments A0 and A5, and the minimum stress locates in the middle of the bridge at the end spines. The maximum stress of steel rails is 150 MPa under high-level earthquakes, which is much smaller than its design yield stress of 500 MPa. This means that the steel rails are still in an elastic state, and no damage has occurred. The reason is that the fasteners connecting the track plates to the rails are longitudinal slidable. Taken together, the overall stress responses of longitudinal continuous components in track structure are basically the same for the three considered cases, with no major differences, which also illustrates that the adoption of the SSDFB will not have adverse effects on

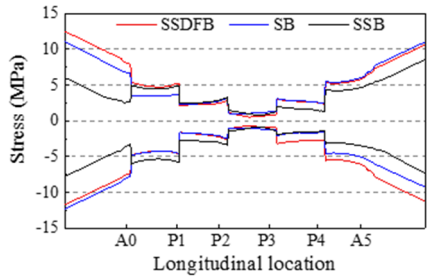

(a) Sliding layer under earthquake G1

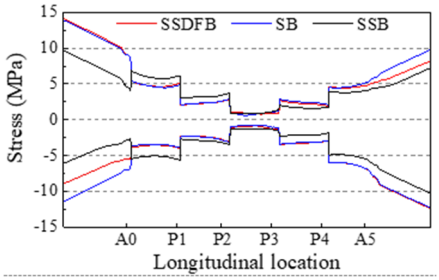

(b) Sliding layer under earthquake G2

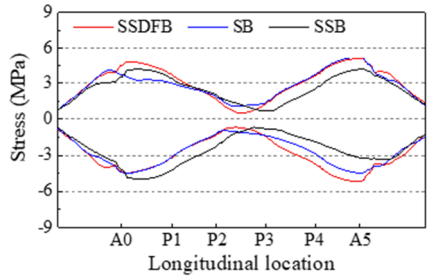

(c) Shear groove under earthquake G1

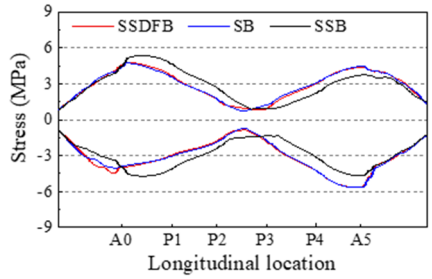

(d) Shear groove under earthquake G2

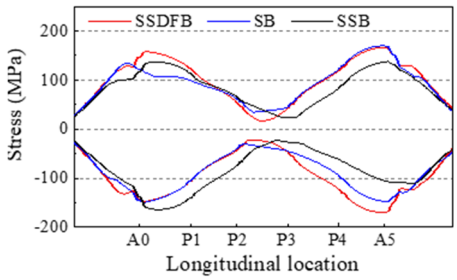

(e) Rail under earthquake G1

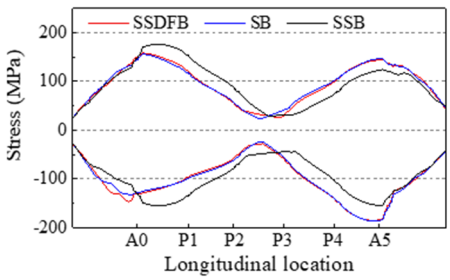

(f) Rail under earthquake G2

Fig. 30 Peak stress of longitudinal continuous components under earthquakes

the longitudinal components of track structure.

6. Conclusions

In this study, an innovative hybrid isolate bearing is proposed by combining the spherical bearing and the S-shaped steel damper. First, the mechanical behavior of SSDFB was thoroughly investigated based on their physical composition and the theoretical equations were derived. Then by comparing with SSD's experimental and theoretical results, the accuracy of the FE model was verified. Based on the established numerical model, the influences of key bearing parameters on the SSDFB mechanical characteristics were investigated. The seismic performance of the SSDFB isolated bridge was evaluated through a detailed comparison of the seismic responses with those from responses of bridges with normal spherical bearing and spherical bearing with strengthened shear keys. The following conclusions can be drawn:

- The proposed SSDFB combines the friction and steel elastoplastic deformation of energy dissipation methods with good energy dissipation capacities. In normal working stages, the SSDs can provide stiffness against service loads; and during the case of medium and large earthquakes, the steel dampers are to yield and dissipates seismic energy by hysteretic behavior. At large displacement, the SSDFB appears to have a significant stiffness strengthening stage with a large secondary stiffness and function as a bridge restrainer.
- The number and dimensions of S-shaped steel plate, friction coefficient of AFS, and gap length are the key parameters that affect the deformation ability and mechanical behaviors of SSDFBs. Reasonable values can be determined during the iteration design according to performance targets of the track-bridge structure, which can be adapted to different bridge structures and different levels of seismic demand.
- The SSDFB enhances energy dissipation capacity of the HSR bridge-track structure and the peak displacements of movable bearing are limited. Besides, the SSDFB can effectively restrain the girder displacement and prevent the occurrence of bridge unseating or collision due to the bearing's large second stiffness. For the substructure, the SSDFB significantly reduces the pier-top displacement and shear force responses under earthquakes, avoiding piers entering the yielding stage. The residual displacements of piers are also reduced by the SSDFB.
- The seismic control effects of SSDFB for track structure are different due to the complex coupling between track components. The SSDFBs can largely reduce peak responses of the connection components of track structure, such as sliding layer and shear grooves but have a small control effect on CA mortar layer, track plate and rails. At the same time, there are non-significant amplification effect of most structural responses due to the isolation of SSDFBs.
- It is worth noting that the vertical force applied to the SSDFBs is a constant value under an earthquake based on the assumption that the effect of the inertia force caused by vertical earthquakes was neglected. However, the SSDFBs are sensitive to vertical loading due to the friction components. The seismic responses of the bridge-track structure may be different when considering large vertical earthquakes. Therefore, further investigation needed to be conducted to emphasize the influence of vertical earthquakes.
- Since only the SSDs were experimentally investigated in this study, the experimental study of the entire SSDFB bearing specimen should be proceeded in the future. More accurate finite element models, for example considering low cycle fatigue damage, can also be implemented.

Acknowledgments

The authors are grateful for the financial support from the National Natural Science Foundation of China (Project No. 51878563, 52022113) and the Fundamental Scientific Research Expenses of IME, China Earthquake Administration (Project No. 2020EEEVL0403). Any opinions, findings, conclusions, or recommendations expressed in this paper are those of the authors.

References

AASHTO (2014), Guide specifications for seismic isolation design, American Association of State Highway and Transportation Officials, Washington, D.C., USA.

FEMA 461 (2000), Interim testing protocols for determining the seismic performance characteristics of structural and nonstructural components, American Application Technology Council, USA.

Feng, D.M., Li, A.Q. and Guo, T. (2020), "Seismic control of a single-tower extradosed railway bridge using the E-Shaped steel damping bearing", *Soil Dyn. Earthq. Eng.*, **136**, p. 106249. https://doi.org/10.1016/j.soildyn.2020.106249

Filipov, E.T., Revell, J.R., Fahnestock, L.A., LaFave, J.M., Hajjar, J.F., Foutch, D.A. and Steelman, J.S. (2013), "Seismic performance of highway bridges with fusing bearing components for quasi-isolation", *Earthq. Eng. Struct. Dyn.*, **42**, 1375-1394. https://doi.org/10.1002/eqe.2277

GB 50111 (2006), Code for seismic design of railway engineering, China National Railway Administration, Beijing, China. [In Chinese]

GB/T 1591 (2008), High strength low alloy structural steels, Ministry of Housing and Urban-Rural Development of the People's Republic of China, Beijing, China. [In Chinese]

Guan, Z., Li, J. and Xu, Y. (2010), "Performance test of energy dissipation bearing and its application in seismic control of a long-span bridge", *J. Bridge Eng.*, **15**(6), 622-630.

Guo, J.J., Zhong, J. and Dang, X.Z. (2017), "Seismic performance assessment of a curved bridge equipped with a new type spring restrainer", *Eng. Struct.*, **151**, 105-114. https://doi.org/10.1016/j.engstruct.2017.08.006

Guo, W., Hu, Y. and Gou, H. (2020a), "Simplified seismic model of CRTS II ballastless track structure on high-speed railway bridges in China", *Eng. Struct.*, **211**, 110453.

https://doi.org/10.1016/j.engstruct.2020.110453
Guo, W., Du, Q. and Huang, Z. (2020b), "An improved equivalent energy-based design procedure for seismic isolation system of simply supported bridge in China's high-speed railway", *Soil Dyn. Earthq. Eng.*, **134**, 106161. https://doi.org/10.1016/j.soildyn.2020.106161
Guo, W., Hu, Y. and Hou, W. (2020c), "Seismic damage mechanism of CRTS-II slab ballastless track structure on high-speed railway bridges", *Int. J. Struct. Stabil. Dyn.*, **20**(01), 2050011. https://doi.org/10.1142/S021945542050011X
Guo, W., Wang, Y., Liu, H., Long, Y., Jiang, L. and Yu, Z. (2021), "Running safety assessment of trains on bridges under earthquakes based on spectral intensity theory", *J. Struct. Stabil. Dyn.*, **14**, 2140008. https://doi.org/10.1142/S0219455421400083
Guo, W., Wang, Y., Zeng, C., Wang, T., Gu, Q., Zhou, H., Zhou, L. and Hou, W. (2022), "Moving Safety Evaluation of High-speed Train on Post-earthquake Bridge Utilizing Real-time Hybrid Simulation", *J. Earthq. Eng.*, 1-30. https://doi.org/10.1080/13632469.2021.1999869
He, X., Kawatani, M. and Hayashikawa, T. (2011), "Numerical analysis on seismic response of Shinkansen bridge-train interaction system under moderate earthquakes", *Earthq. Eng. Eng. Vib.*, **10**(1), 85-97. https://doi.org/10.1007/s11803-011-0049-1
He, X., Wu, T., Zou, Y., Chen, Y. F., Guo, H. and Yu, Z. (2017), "Recent developments of high-speed railway bridges in China", *Struct. Infrastr. Eng.*, **13**(12), 1584-1595. https://doi.org/10.1080/15732479.2017.1304429
He, W.K., Jiang, L., Wei, B. and Wang, Z.W. (2021), "Influence of pier height on the effectiveness of seismic isolation of friction pendulum bearing for single-track railway bridges", *Smart Struct. Syst., Int. J.*, **28**(2), 213-228. https://doi.org/10.12989/sss.2021.28.2.213
Hwang, Y., Lee, C.W. and Jung, H.J. (2020), "Feasibility of a new hybrid base isolation system consisting of MR elastomer and roller bearing", *Smart Struct. Syst., Int. J.*, **25**(3), 323-335. https://doi.org/10.12989/sss.2020.25.3.323
Jangid, R.S. and Kelly, J.M. (2001), "Base isolation for near-fault motions", *Earthq. Eng. Struct. Dyn.*, **30**(5), 691-707. https://doi.org/10.1002/eqe.31
Jiang, L., Cao, S. and Wei, B. (2019), "Effects of friction-based fixed bearings on seismic performance of high-speed railway simply supported girder bridges and experimental validation", *Adv. Struct. Eng.*, **22**(3), 687-701. https://doi.org/10.1177/1369433218798120
Kang, X., Jiang, L. and Yu, B. (2017), "Seismic damage evaluation of high-speed railway bridge components under different intensities of earthquake excitations", *Eng. Struct.*, **152**(1), 116-128. https://doi.org/10.1016/j.engstruct.2017.08.057
Kawashima, K., Unjoh, S, and Hoshikuma, J.I. (2011), "Damage of bridges due to the 2010 Maule, Chile, earthquake", *J. Earthq. Eng.*, **15**(7), 1036-1068. https://doi.org/10.1080/13632469.2011.575531
Li, J.Z., Peng, T.B. and Yan, X. (2008), "Damage investigation of girder bridges under the Wenchuan earthquake and corresponding seismic design recommendations", *Earthq. Eng. Eng. Vib.*, **7**, 337-344. https://doi.org/10.1007/s11803-008-1005-6
Li, S., Dezfuli, and Farshad, H. (2018), "Displacement-based seismic design of steel, FRP, and SMA cable restrainers for isolated simply supported bridges", *J. Bridge Eng.*, **23**(6), p. 04018032.
Li, H., Yu, Z. and Mao, J. (2021), "Effect of seismic isolation on random seismic response of High-Speed railway bridge based on probability density evolution method", *Structures*, **29**, 1032-1046. https://doi.org/10.1016/j.istruc.2020.11.070
Lin, T.K., Lu, L.Y. and Chen, C.J. (2018), "Semi-active leverage-type isolation system considering minimum structural energy", *Smart Struct. Syst., Int. J.*, **21**(3), 373-387. https://doi.org/10.12989/sss.2018.21.3.373
Luo, X. (2005), "Study on methodology for running safety assessment of trains in seismic design of railway structures", *Soil Dyn. Earthq. Eng.*, **25**, 79-91. https://doi.org/10.1016/j.soildyn.2004.10.005
Mahdi, U., Ali, R. and Mojtaba, A. (2021), "Steel dual-ring dampers: Micro-finite element modelling and validation of cyclic behavior", *Smart Struct. Syst., Int. J.*, **28**(4), 579-592. https://doi.org/10.12989/sss.2021.28.4.579
Martinez, M.D. and Filiatrault, A. (2015), "A case study on the application of passive control and seismic isolation techniques to cable-stayed bridges: A comparative investigation through non-linear dynamic analyses", *Eng. Struct.*, **99**, 232-252. https://doi.org/10.1016/j.engstruct.2015.04.048
Mohsen, K., Aghdas, A., Sadjad, G. and Seyyed, R.S. (2021), "An efficient approach for optimum shape design of steel shear panel dampers under cyclic loading", *Smart Struct. Syst., Int. J.*, **27**(3), 547-557. https://doi.org/10.12989/sss.2021.27.3.547
Ozbulut, O.E. and Hurlebaus, S. (2011), "Optimal design of superelastic-friction base isolators for seismic protection of highway bridges against near-field earthquakes", *Earthq. Eng. Struct. Dyn.*, **40**, 273-291. https://doi.org/10.1002/eqe.1022
Park, R. (1988), "State of the art report ductility evaluation from laboratory and analytical testing", *Proceedings of Ninth World Conference on Earthquake Engineering*, Tokyo-Kyoto.
Patrick, T., James, K. and Tan, O. (2017), "Design approach of high damping rubber bearing for seismic isolation", *Smart Struct. Syst., Int. J.*, **20**(3), 303-309. https://doi.org/10.12989/sss.2017.20.3.303
Qu, B., Dai, C. and Qiu, J. (2019), "Testing of seismic dampers with replaceable U-shaped steel plates", *Eng. Struct.*, **179**, 625-639. https://doi.org/10.1016/j.engstruct.2018.11.016
Raheem, S. (2009), "Pounding mitigation and unseating prevention at expansion joints of isolated multi-span bridges", *Eng. Struct.*, **31**(10), 2345-2356. https://doi.org/10.1016/j.engstruct.2009.05.010
Shao, G., Jiang, L. and Chouw, N. (2014), "Experimental investigations of the seismic performance of bridge piers with rounded rectangular cross-sections", *Earthq. Struct., Int. J.*, **7**(4), 463-484. https://doi.org/10.12989/eas.2014.7.4.463
Sheikhi, J., Fathi, M. and Rahnavard, R. (2021), "Numerical analysis of natural rubber bearing equipped with steel and shape memory alloys dampers", *Structures*, **32**, 1839-1855. https://doi.org/10.1016/j.istruc.2021.03.115
Shen, X., Wang, X., Ye, Q. and Ye, A. (2017), "Seismic performance of transverse steel damper seismic system for long span bridges", *Eng. Struct.*, **141**, 14-28. https://doi.org/10.1016/j.engstruct.2017.03.014
TB 10621 (2014), Code for Design of High Speed Railway, China National Railway Administration, Beijing, China. [In Chinese]
Usefvand, M., Rousta, A.M., Azandariani, M.G. and Abdolmaleki, H. (2021), "Steel dual-ring dampers: Micro-finite element modelling and validation of cyclic behavior", *Smart Struct. Syst., Int. J.*, **28**(4), 579-592. https://doi.org/10.12989/sss.2021.28.4.579
Wei, B., Yang, T. and Jiang, L. (2017), "Effects of friction-based fixed bearings on the seismic vulnerability of a high-speed railway continuous bridge", *Adv. Struct. Eng.*, **21**(5), 643-657. https://doi.org/10.1177/1369433217726894
Xiang, N. and Li, J. (2016), "Seismic performance of highway bridges with different transverse unseating-prevention devices", *J. Bridge Eng.*, **21**(9), 04016045.
Yang, T.Y., Tung, D.P. and Li, Y. (2018), "Equivalent energy design procedure for earthquake resilient fused structures",

Earthq. Spectra, **34**(2), 795-815. https://doi.org/10.1193/122716EQS254M

Yuan, W., Wang, B., Cheung, P., Cao, X. and Rong, Z. (2012), "Seismic performance of cable-sliding friction bearing system for isolated bridges", *Earthq. Eng. Eng. Vib.*, **11**, 173-183. https://doi.org/10.1007/s11803-012-0108-2

Zhai, W. and Xia, H. (2001), *Train-Track-Bridge Dynamic Interaction*: *Theory and Engineering Application*, Science Press, China.

Zhai, Z.P., Guo, W. and Yu, Z. (2020), "Experimental and numerical study of S-shaped steel plate damper for seismic resilient application", *Eng. Struct.*, **221**, 111006. https://doi.org/10.1016/j.engstruct.2020.111006

Zou, S., Wenliuhan, H. and Zhou, F.L. (2019), "Shaking table test of a high-speed railway bridge with a new isolation system", *Eng. Struct.*, **196**, 109315. https://doi.org/10.1016/j.engstruct.2019.109315

BS